Laser and Particle Beams (2008), *26*, 433–448. Printed in the USA.

doi:10.1017/S026303460800044X

RAPCAL code: A flexible package to compute radiative properties for optically thin and thick low and high-Z plasmas in a wide range of density and temperature

R. RODRÍGUEZ,[1,2] R. FLORIDO,[1,2] J.M. GIL,[1,2] J.G. RUBIANO,[1,2] P. MARTEL,[1,2] AND E. MÍNGUEZ[2]

[1]Physics Department, University of Las Palmas de Gran Canaria, Las Palmas de Gran Canaria, Spain
[2]Nuclear Fusion Institute-Denim, Polytechnic University of Madrid, Madrid, Spain

(Received 30 May 2008; Accepted 15 June 2008)

Abstract

Radiative properties are fundamental for plasma diagnostics and hydro-simulations. For this reason, there is a high interest in their determination and they are a current topic of investigation both in astrophysics and inertial fusion confinement research. In this work a flexible computation package for calculating radiative properties for low and high Z optically thin and thick plasmas, both under local thermodynamic equilibrium and non-local thermodynamic equilibrium conditions, named RAPCAL is presented. This code has been developed with the aim of providing accurate radiative properties for low and medium Z plasmas within the context of detailed level accounting approach and for heavy elements under the detailed configuration accounting approach. In order to show the capabilities of the code, there are presented calculations of some radiative properties for carbon, aluminum, krypton and xenon plasmas under local thermodynamic and non-local thermodynamic equilibrium conditions.

Keywords: LTE condition; NLTE condition; Optically thick plasmas; Optically thin plasma; Radiative properties

1. INTRODUCTION

Radiative properties of hot dense plasmas remain a subject of current interest (Alexiou *et al.*, 1997; Csanak & Daughton, 2004; Orlov *et al.*, 2007) since they play an important role in the inertial fusion confinement (ICF) research as well as studies in stellar physics (Bauche *et al.*, 2006). In particular, the understanding of ICF plasmas requires emissivities and opacities both for hydro-simulations and diagnostics (Peyrusse, 2004) since, for example, the emission spectra from plasmas under non-local thermodynamic equilibrium (NLTE) may be used for plasma diagnostics, or the spectrally integrated emissivity may be used to determine the evolution of the electronic and radiation temperatures in a hydrodynamic simulation (Bowen *et al.*, 2003). Furthermore, modeling of the energy transport in hot dense plasmas relies on radiative opacities (Yuan *et al.*, 2003; Mínguez *et al.*, 2005).

The first step on the calculation of plasma radiative properties is the computation of the required atomic data. However, this is a complex task since the number of the atomic levels involved, and therefore the amount of atomic data to obtain is huge and approximations must be made. For low and intermediate Z-plasmas detailed level accounting (DLA) or detailed term accounting (DTA) models are commonly used. On the other hand, for high-Z elements statistical approaches involving grouping of levels such as the detailed configuration accounting (DCA) approach or super configuration accounting (SCA) approach (Bar-Shalom *et al.*, 1997; Peyrusse, 2001) have shown to be very efficient when it is combined with unresolved transition array (UTA/SOSA) (Bauche *et al.*, 1987) and/or the super transition array (STA) formalisms (Bar-Shalom *et al.*, 1989). Nowadays, new hybrid models that mix detailed levels and configurations are under development (Mazevet & Abdallah, 2006; Hansen *et al.*, 2007).

Once the atomic data are available, we need to compute the atomic level populations in the plasma. The need for accurate computation of radiative properties covers an extensive range of thermodynamic conditions. Depending on the LTE or NLTE character of the plasma under analysis, existing physics models have different uses or implementations (Peyrusse, 2004). Under LTE conditions there exists an equation which gives the occupation probabilities of bound

Address correspondence and reprint requests to: Rafael Rodríguez, Physics Department, University of Las Palmas de Gran Canaria, Campus Universitario de Tafira, 35017 Las Palmas de Gran Canaria, Spain. E-mail: rrodriguez@dfis.ulpgc.es

states, the Saha-Boltzmann equation, and, moreover, the Kirchoff's gives a simple relationship between the emissivity and the opacity. Therefore, it is only necessary to calculate the opacity from its definition. On the other hand, under NLTE conditions, the problem shows great complexity because there is not an *a priori* expression for the occupation probabilities of bound states, and therefore one must find the statistical distribution of the ionic states by using the so-called collisional-radiative model (CRM), which implies to solve a set of rate equations, with coupling of configurations, free electrons and photons. Moreover, if we consider that for accurate simulations of the emission and the absorption spectra, it is essential to take into account as many quantum levels as possible, and that the Kirchoff's law is no longer valid in this regime and then the opacity and the emissivity must be calculated on the same footing, sometimes the calculations become unmanageable. For this reason, it results that it is more complex to provide accurate level populations under NLTE than LTE conditions.

Due to the difficulties that arise in the calculation of the radiative properties there is still a lack of complete understanding of these magnitudes and since they are relevant in many areas of the plasma, many groups are currently developing codes and calculations (Serduke *et al.*, 2000; Peyrusse, 2001; Bar-Shalom *et al.*, 2001; Bowen, 2001; Zeng & Yuan, 2002; Iglesias *et al.*, 2003; Bowen *et al.*, 2003; Yuan *et al.*, 2003; Rubiano *et al.*, 2004; Chung *et al.*, 2005; Hakel *et al.*, 2006; Wu *et al.*, 2006; Yuan & Moses, 2006; Mazevet & Abdallah, 2006; Rodríguez *et al.*, 2006; Abdallah *et al.*, 2007*a*, 2007*b*; Hansen *et al.*, 2007) of plasma radiative properties and new results are always welcomed.

In this paper, a new code is presented, RAPCAL, for calculating radiative properties such as opacities, emissivities, source functions, intensities, transmissions, and radiative power losses for optically thin and thick plasmas, both under LTE and NLTE conditions. The next section is devoted to describing RAPCAL code, in the third section, some results are presented in order to check the validity of the model and finally, some conclusions and general remarks are presented.

2. CODE DESCRIPTION

RAPCAL is an extension of the analytical expressions based kinetics (ABAKO) code (Florido, 2007; Florido *et al.*, 2008) designed for the calculation of plasma radiative properties. It is divided in three modules. The first one was designed to calculate the required atomic data. The second one is devoted to the calculation of the population of optically thin and thick plasmas, both under LTE and NLTE conditions. And, finally, in the third module, radiative properties are calculated for both plasma regimes. In the following, we will describe these modules.

2.1. Atomic Module

RAPCAL contains an internal model to generate atomic magnitudes but it has also been designed to work using external data coming from other computational codes or databases.

At the present time, the external source often used in RAPCAL is the flexible atomic code (FAC) (Gu, 2003), which is able to provide atomic data either in DLA or relativistic DCA approaches. The energy of the levels or configurations of an atomic ion with N electrons are obtained by diagonalizing the relativistic Hamiltonian. The basis states which are usually referred to as configuration state functions (CSF), which are built as anti-symmetric sums of products of N one-electron Dirac spinners. In coupling the angular momenta, the standard *jj*-coupling scheme is used. Finally, the approximate atomic wave functions are evaluated mixing the basis states (configuration interaction, CI) with the same symmetries with the mixing coefficients obtained from diagonalizing the total Hamiltonian.

With respect to the atomic model implemented in RAPCAL, this always works in the DCA approach. In this case, for a given ion, for each relativistic configuration, we solve a Dirac equation for each occupied level which gives us its relativistic mono-electronic wave function, and the corresponding energy level. The total energy is then obtained using a density-functional formalism (Rajagopal, 1980; Kohn & Sham, 1965) assuming the local density approach for the exchange and correlation energy. The effective potential used in the Dirac equation is anyone of the analytical central ones developed by our group. These can model isolated ions (Martel *et al.*, 1995)

$$U^0(r) = -\frac{1}{r}\{(N-1)\phi(r) + Z - N + 1\}, \tag{1}$$

where N is the number of bound electrons and Z is the nuclear charge and $\phi(r)$ is the screening function, given by

$$\phi(r) = \begin{cases} e^{-a_1 r^{a_3}} & \text{if } N \geq 12 \\ (1-a_2)e^{-a_1 r} & \text{if } 8 \leq N \leq 11 \text{ or } N = 2, 3, \\ e^{-a_1 r} & \text{if } 4 \leq N \leq 7 \end{cases} \tag{2}$$

where the three parameters a_1, a_2, a_3 were determined by fitting the potential (Martel *et al.*, 1998) to a self-consistent one used in DAVID code (Liberman *et al.*, 1971). Ions immersed into weakly (Gil *et al.*, 2002) and strongly coupled plasmas (Rodriguez *et al.*, 2007) are also modeled by potentials $U^I(r)$ and $U^{II}(r)$, respectively

$$U^{II}(r) = -\frac{1}{r}\Big\{(N-1)(\phi(r) - \eta(r)) + 1\Big\} - \frac{1}{r}\Big[Z - N + (N-1)\eta(0)\Big]e^{-ar}, \tag{3}$$

with

$$\eta(r) = \frac{1}{2}a\int_0^\infty e^{-a|s-r|}\phi(s)ds, \tag{4}$$

https://doi.org/10.1017/S026303460800044X Published online by Cambridge University Press

$$U^{II}(r) = U^0(r) - U^0(R_0) - \frac{\bar{Z}}{2R_0}\left(\frac{r}{R_0}\right)^2 + \frac{\bar{Z}}{2R_0}, \quad (5)$$

where $\bar{Z}$ is the plasma average ionization, R_0 is the ion-sphere radius, and a is the inverse of the Debye radius. Both for isolated and non-isolated situations, singly and doubly excited configurations can be included (Rodriguez *et al.*, 2002). The usefulness and accuracy of this set of analytical potentials in obtaining atomic data for level populations and opacities have been shown previously (Minguez *et al.*, 1998, 2005; Bowen *et al.*, 2006; Rubiano *et al.*, 2007). Furthermore, this atomic model is a very useful tool in order to optimize detailed calculations since it provides us in a very short time with valuable information such as the plasma average ionization and the most abundant ions in the plasma for given conditions. We would like to point out that this atomic module is also ready to perform the atomic calculations with other analytical potentials available in the literature or using a self-consistent potential (Liberman *et al.*, 1971) and it is also implemented a relativistic screened hydrogenic model (Rubiano *et al.*, 2004) for the situations wherein very fast atomic calculations are desired, for example in-line hydro-code calculations.

Finally, for dense plasmas, either for the calculations using FAC or the atomic model, the lowering of the ionization potential is taken into account following the model proposed by Stewart and Pyatt (1966)

$$\Delta I_i = \frac{3}{2}\frac{(\xi_i + 1)e^2}{R_0}\left\{\left[1 + \left(\frac{D}{R_0}\right)^3\right]^{2/3} - \left(\frac{D}{R_0}\right)^2\right\}, \quad (6)$$

where D is the Debye length, e is the electron charge, and ξ_i is the charge of the ion, i. When the atomic data are calculated using the analytical potential including plasma effects, the atomic, and the population calculation modules must be solved iteratively until the convergence is achieved.

2.2. Plasma Population Distribution Calculation Module

This module of RAPCAL is basically an ABAKO code (Florido, 2007; Florido *et al.*, 2008). At the moment, the code works under stationary assumption. Therefore, to find the level population it solves the set of steady-state rate equations

$$\sum_{\xi' m'} N_{\xi' m'} R^{+}_{\xi' m' \to \xi m} - \sum_{\xi' m'} N_{\xi m} R^{-}_{\xi m \to \xi' m'} = 0, \quad (7)$$

where $N_{\xi m}$ denotes the population density of the atomic level ξm and $R^{+}_{\xi' m' \to \xi m}$ and $R^{-}_{\xi m \to \xi' m'}$ take into account all the processes which contribute to populate and depopulate the ξm state, respectively. The collisional-radiative steady-state (CRSS) model in ABAKO is solved level by level (or configuration by configuration, depending on the DLA or DCA approach) and it is applied to low-to-high Z ions under a wide range of laboratory or astrophysical plasma conditions: corona equilibrium, NLTE, or LTE, optically thin and thick plasmas. Special care was taken during the development of our CRSS model to achieve an optimal equilibrium between accuracy and computational cost. Hence, analytical expressions has been employed for the rate coefficients of the atomic processes included in the CRSS model, which yield a substantial saving of computational requirements, but providing satisfactory results in relation to those obtained from more sophisticated codes and experimental data.

The processes included in the CRSS model are the following: collisional ionization (Lotz, 1968) and three-body recombination, spontaneous decay, collisional excitation (Van Regemorter, 1962), and deexcitation, radiative recombination (Kramers, 1923), electron capture and auto-ionization. We have added between brackets the references wherefrom their approximated analytical rates coefficients have been acquired. The rates of the inverse processes are obtained through the detailed balance principle. It is worth pointing out that the auto-ionizing states are included explicitly. It has been proved that their contribution is critical in the determination of the ionization balance. The cross section of the auto-ionization is evaluated using detailed balance principle from the electron capture cross section. This one is obtained from the collisional excitation cross section using a known approximation (Griem, 1997). Only those atomic processes whose rates are independent of the radiation field intensity are explicitly considered in the CRSS model.

RAPCAL also models homogeneous optically thick plasmas. For this situation, the escape factor formalism (Mancini *et al.*, 1987) for the basic geometries—plane, cylindrical and spherical—is used in order to take into account the bound-bound opacity effects. Nowadays, this module is being improved to model non-uniform plasmas with planar geometry using a new technique for the line transport (Florido *et al.*, 2006) based on the definition of zone-to-zone radiative coupling coefficients. A full description of this formalism will be exposed in a forthcoming paper.

Finally, since the number of rate equations is huge due to the number of atomic levels involved, we employ the technique of sparse matrices to storage the non-zero elements of the coefficient matrix of the system, which implies substantial savings in memory requirement. For the matrix inversion we use iterative procedures (Florido *et al.*, 2005) because they entail much less memory than direct methods and they are also faster. It is worth remarking this fact because, as we said previously, when we include plasma effects through the continuum lowering in our atomic model this module and the atomic one must be solved iteratively.

2.3. Radiative Properties Calculation Module

The total spectrally resolved opacity and emissivity of plasma is the combination of bound-bound, bound-free, free-free, and scattering processes. Besides stimulated emission

https://doi.org/10.1017/S026303460800044X Published online by Cambridge University Press

is taken into account. The bound-bound absorption coefficient and emissivity are evaluated through the following equations

$$\mu_{bb}(\nu) = \sum_{\xi} \sum_{i,j} \mu_{\xi_{i,j}}(\nu), \tag{8}$$

$$j_{bb}(\nu) = \sum_{\xi} \sum_{i,j} j_{\xi_{j,i}}(\nu), \tag{9}$$

where

$$\mu_{\xi_{i,j}}(\nu) = \frac{\pi}{mc}\left(\frac{e^2}{4\pi\varepsilon_0}\right) N_{\xi_i} f_{\xi_{i,j}} \phi^a_{\xi_{i,j}}(\nu)\left[1 - \frac{N_{\xi_j} g_{\xi_j}}{N_{\xi_j} g_{\xi_i}}\right], \tag{10}$$

$$j_{\xi_{j,i}}(\nu) = h\nu^3 N_{\xi_j}\left(\frac{e^2}{2mc^3\varepsilon_0}\right)\frac{g_{\xi_i}}{g_{\xi_j}} f_{\xi_{i,j}} \phi^a_{\xi_{i,j}}(\nu), \tag{11}$$

where m is the electron mass, c is the speed of the light, i and j denote levels of ion ξ, $N_{\xi i}$ denotes the population (cm^{-3}) of the i-level of this ion, ν is the frequency of the photon, g denotes the degeneracy of the level, and $f_{\xi_{i,j}}$ denotes the oscillator strength of the transition, which is evaluated in the electric dipole approximation as it follows

$$f_{\xi_{i,j}} = \frac{E_j - E_i}{3(2J+1)} \left|\langle \Psi_j \| \mathbf{P}^{(1)} \| \Psi_i \rangle\right|^2, \tag{12}$$

where $\mathbf{P}^{(1)}$ is the electron dipole operator. When it is employed, the atomic model implemented in RAPCAL, the oscillator strength associated to the transition between two relativistic configurations i and j is evaluated in terms of mono-electronic oscillator strengths (Rodriguez *et al.*, 2007). In Eq. (11), $\phi^a_{\xi_{i,j}}(\nu)$ and $\phi^e_{\xi_{j,i}}(\nu)$ are the absorption and the emission line-shape functions, respectively. In this work, both profiles have been taken as equal, assuming complete redistribution hypothesis (Mihalas, 1978). In our work, we have considered natural, Doppler, and electron-impact broadenings. The Doppler half width at half maximum (HWHM) is given by Cowan (1981)

$$\Gamma_d = 3.858 \times 10^{-5} (kT/A)^{1/2} (h\nu_{ij}), \tag{13}$$

where A is the atomic weight of the ion in grams, and kT (with k the Boltzmann constant and T the electron temperature), $h\nu_{ij}$ (the transition energy), and Γ_d are in eV. The calculation of the electron-impact HWHM is somewhat complicated and it can be obtained by fully quantum mechanical calculation (Seaton, 1990) or by semi-classical method (Griem, 1974), but even the semi-classical method needs elaborate calculation and it is not useful to obtain a large number of such data for the evaluation of the X-ray spectra (Zeng *et al.*, 2001*a*). Expressed using a semi-empirical formula (Dimitrijevic & Konjevic, 1980, 1987) the electron–impact HWHM in eV is given by

$$\Gamma_l = N_e \frac{8\pi}{6}\frac{\hbar^2}{m^2}\left(\frac{2m}{\pi kT}\right)^{1/2}\frac{\pi}{\sqrt{3}}\left(0.9 - \frac{1.1}{\xi+1}\right) \times \sum_{j=i,f}\left(\frac{3n_j}{2(\xi+1)}\right)^2\left(n_j^2 - l_j^2 - l_j - 1\right), \tag{14}$$

where N_e is the electron density and n_i, n_j, l_i, l_j are the principal and angular quantum numbers of the initial and final orbitals, respectively, related with the transition. In this paper, the width due to collisions between ions has not been considered. Zeng and Yuan (2002) have verified that the semi-empirical formula given in Eq. (14) provides results very similar to those of a quantum mechanical calculation. The line-shape function is applied with the Voigt profile which includes all the broadenings cited before

$$\phi(\nu) = \frac{\sqrt{\ln 2}}{\sqrt{\pi} h \Gamma_d} H(a, \nu), \tag{15}$$

$$H(a,s) = \frac{a}{\pi}\int_{-\infty}^{+\infty} \frac{e^{-x^2}}{a^2 + (s-x)^2} dx, \tag{16}$$

where $a = \sqrt{\ln 2}(\Gamma_l + \Gamma_n)/\Gamma_d$, Γ_n is the natural HWHM, and $s = \sqrt{\ln 2}(h\nu - h\nu_{ij})/\Gamma_d$. The natural and electron-impact HWHM have been added since in the impact approximation, the two contributions have the same Lorentz profile shape.

For the bound-free transitions, the absorption coefficient and the emissivity are evaluated as follows

$$\mu_{bf}(\nu) = \sum_{\xi,i}\sum_{\xi+1,j} \mu_{\xi_i,\xi+1_j}(\nu), \tag{17}$$

$$j_{fb}(\nu) = \sum_{\xi+1,j}\sum_{\xi,i} j_{\xi+1_j,\xi_i}(\nu), \tag{18}$$

where

$$\mu_{\xi_i,\xi+1_j}(\nu) = N_{\xi_i}\sigma(\nu)_{\xi_i,\xi+1_j}\left[1 - \frac{N_{\xi+1_j} g_{\xi_i}}{N_{\xi_i} g_{\xi+1_j}}\right] N_e n(\varepsilon, T), \tag{19}$$

$$j_{\xi+1_j,\xi_i}(\nu) = \frac{h\nu^3}{2\pi}\left(\frac{h^2}{2m}\right)^{3/2}\frac{g_{\xi_i}}{g_{\xi+1_j}}\varepsilon^{1/2} N_{\xi+1_j}\sigma(\nu)_{\xi_i,\xi+1_j} N_e f(\varepsilon, T), \tag{20}$$

where $n(\varepsilon, T)$ is the free electron distribution, ε is the free electron energy, $f(\varepsilon, T) = g(\varepsilon)n(\varepsilon, T)$ where $g(\varepsilon)$ is the free electron degeneracy and $\sigma(\nu)_{\xi_i,\xi+1_j}$ is the photoionization cross section. In Eq. (20), the Milne relation has been considered. When using the FAC code for generating the atomic data, the photoionization cross section is calculated in the distorted wave (DW) approximation without including resonances, improving the efficiency of the calculations by

https://doi.org/10.1017/S026303460800044X Published online by Cambridge University Press

extending the factorization-interpolation procedure of Bar-Shalom *et al.* (1988) to the evaluation of the photoionization cross section. Thus, the photoionization cross section is given in terms of the differential strength, in atomic units (Gu, 2003)

$$\sigma(\nu)_{\xi_i,\xi+1_j} = 2\pi\alpha \frac{1+\alpha^2\varepsilon}{1+0.5\alpha^2\varepsilon} \frac{df_{\xi_i,\xi+1_j}}{d\varepsilon}, \tag{21}$$

where α is the fine structure constant, and the differential oscillator strength may be calculated similarly to the bound-bound oscillator strength. When the atomic data are calculated using the atomic model implemented in the code, the cross section is computed using the Kramer expression (Kramers, 1923)

$$\sigma(\nu)_{\xi_i,\xi+1_j} = \frac{64\pi a_0^2 n_i \alpha}{3^{3/2}(\xi_i+1)} \left(\frac{E_{n\xi_i}}{\varepsilon}\right)^3, \tag{22}$$

where a_0 is the Bohr radius and $E_{n\xi_i}$ is the threshold ionization energy for the shell n_i of the ion ξ in the electronic configuration i.

For the free-free transitions, the absorption coefficient has been evaluated using the semi-classical expressions of Kramer for the cross section (Rose, 1992)

$$\sigma_{ff}(\nu) = \frac{16\pi^2 e^2 h^2 \alpha}{3\sqrt{3}(2\pi m)^{3/2}} \frac{\bar{Z}^2 N_e}{(kT)^{1/2}(h\nu)^3} g_{ff}, \tag{23}$$

where the free-free Gaunt factor g_{ff} is taken as unit. The total free-free absorption coefficient is

$$\mu_{ff}(\nu) = N_{ion}\sigma_{ff}(\nu)(1-e^{-h\nu/kT}), \tag{24}$$

where N_{ion} is the ion density and the negative term again corrects for induced processes. Eq. (24) is valid for LTE conditions as long as the velocities are maxwellian. The free-free emissivity is also evaluated through the Kramer approximation (Minguez, 1993)

$$j_{ff}(\nu) = \frac{32\pi e^4 a_0^2 \alpha^3 \bar{z}^2}{2\sqrt{3}(2\pi m)^{3/2}\hbar} \left(\frac{m}{2\pi kT}\right)^{1/2} N_e N_{ion} e^{-h\nu/kT}. \tag{25}$$

Finally, the scattering contribution to the absorption is approximated using the Thomson scattering cross section (Rutten, 1995). Thus, the total opacity and emissivity can be written as follows

$$\kappa(\nu) = \frac{1}{\rho}\Big(\mu_{bb}(\nu) + \mu_{bf}(\nu) + \mu_{ff}(\nu) + \mu_{scatt}(\nu)\Big), \tag{26}$$

$$j(\nu) = j_{bb}(\nu) + j_{bf}(\nu) + j_{ff}(\nu), \tag{27}$$

where ρ is the density of matter (gcm^{-3}). The source function is then evaluated through the following expression

$$S(\nu) = \frac{j(\nu)}{\rho\,\kappa(\nu)}. \tag{28}$$

The Rosseland and Planck mean opacities are given by Serduke *et al.* (2000)

$$\frac{1}{\kappa_{Rosseland}} = \int_0^\infty d\nu B'(\nu, T)/\kappa(\nu), \tag{29}$$

$$\kappa_{Planck} = \int_0^\infty d\nu B(\nu, T)[\kappa(\nu) - \kappa_{scatt}(\nu)], \tag{30}$$

where $B'(\nu, T)$ is the temperature derivative of the normalized Planck function $B(\nu, T)$, which is given by

$$B(\nu, T) = \frac{15}{\pi^4 T} \frac{u^3}{e^u - 1}, \tag{31}$$

where $u = h\nu/kT$ is a dimensionless variable. The transmission spectrum, which provides the fraction of radiation transmitted with respect to some incident source of arbitrary intensity, is given by Zeng and Yuan (2002)

$$T(h\nu) = e^{-\rho\kappa(h\nu)L}, \tag{32}$$

where L is the path length transversed by the light source through the plasma.

The radiative power loss, which can be important in understanding energy distributions and spectral characteristics of plasmas, is evaluated as following (eV/s/ion) (Chung *et al.*, 2006) for the bound-bound contribution

$$P_{bb}(T_e, N_e) = \sum_\xi \sum_{ij} h\nu_{ij} A_{ij} N_{\xi_j}, \tag{33}$$

where A_{ij} is the spontaneous decay rate of the transition. For the bound-free contribution, we have

$$P_{bf}(T_e, N_e) = 4\pi \sum_\xi \sum_{ij} N_{\xi_i} \cdot \left[\frac{N_{\xi-1_j} N_\xi}{N_{\xi_i} N_{\xi-1}}\right]^{LTE} \int_{\nu_0}^\infty \sigma(\nu)_{\xi_i,\xi+1_j} \times \left(\frac{2h\nu^3}{c^2}\right) e^{-(h\nu/kT_e)} d\nu, \tag{34}$$

where the LTE population ratio is obtained through the Saha equation and ν_0 is the threshold frequency. The free-free contribution is obtained for a pure Coulomb field as (Karzas & Latter, 1961)

$$P_{ff}(T_e, N_e) = 9.55 \times 10^{-14} N_e T_e^{1/2} \sum_\xi Z_\xi^2 N_\xi, \tag{35}$$

where we have assumed the gaunt factor equal to unity. The total radiative power loss is then obtained as the sum of the

https://doi.org/10.1017/S026303460800044X Published online by Cambridge University Press

Table 1. *Set of configurations and number of relativistic configurations and levels considered in the calculations performed by RAPCAL code for carbon ions ($n \leq 10$, $n' \leq 6$)*

	C-like	B-like	Be-like	Li-like	He-like	H-like
	$(2)^4$	$(2)^3$	$(2)^2$	$(2)^1$	$(1)^2$	$(1)^1$
	$(2)^3$nl	$(2)^2$nl	$(2)^1$nl	nl	$(1)^1$nl	nl
	$(2)^2(3)^2$	$(2)^1(3)^2$	$(3)^2$	$(1)^1(2)^2$	$(2)^2$	
	$(2)^2(3)^1$n'l	$(2)^1(3)^1$n'l	$(3)^1$n'l	$(1)^1(2)^1$n'l	$(2)^1$n'l	
		$(1)^1(2)^4$	$(1)^1(2)^3$	$(1)^1(3)^2$	$(3)^2$	
		$(1)^1(2)^3$n'l	$(1)^1(2)^2$ n'l	$(1)^1(3)^1$n'l	$(3)^1$n'l	
Configs	1677	1299	644	519	352	100
Levels	16616	8871	2789	2642	910	100

three contributions. Finally, the radiative cooling coefficient of an ion can be obtained from the radiative power loss of the ion divided by its number density in the plasma.

3. RESULTS

It is not our aim in this work to carry out an exhaustive study of the radiative properties but rather to present some results that allow us to show the capabilities of the code and also to check the results that it provides with other codes and available experimental data.

We have made calculations in a wide range of plasma conditions, and, therefore, CE, NLTE, and LTE situations are considered. In particular, we have analyzed some interesting radiative magnitudes of plasmas of carbon, aluminum, krypton, and xenon, covering, this way, plasmas of low, intermediate, and high Z. The study of carbon plasmas is a subject of current interest since it is likely to be a major plasma-facing wall component in ITER (Skinner & Federici, 2006) and it plays a major role in inertial fusion scenarios (Filevich *et al.*, 2007). Aluminum has always been considered as a representative of low Z element and much experimental and theoretical effort has been made to investigate the opacities through these plasmas during the past two decades (Zeng & Yuan, 2002; Keskinen & Schmitt, 2007; Lomonosov, 2007) and, therefore, it is a benchmark element. Furthermore, both aluminum and carbon plasmas have interest in astrophysics. Finally, radiation in the outermost region of magnetically confined fusion plasmas from impurities seems to be a possible mechanism for controlling the heat load deposited onto the plasma facing components of a fusion reactor (Fournier *et al.*, 2000; Post, 1995). Noble gases such as krypton and xenon are potentially useful in this regard (Mandrekas *et al.*, 1996) showing the advantage that they do not perturb the plasma core.

For carbon and aluminum plasmas, we have performed calculations both under DLA approach (RAPCAL-DLA), using atomic data from FAC code including CI among levels belonging to the same configuration, and under relativistic DCA approach with atomic data obtained from the atomic module implemented in RAPCAL based on the analytical potential given by Eqs. (1) and (2) (RAPCAL-AP). The comparison of the results will permit us to show the accuracy of the simple atomic model implemented in RAPCAL. Finally, for the krypton and xenon cases, the calculations were carried out in the relativistic DCA approach, using for the former the data provided by the analytical potential and for the latter atomic data obtained from FAC code.

Both the level populations and radiative properties depend strongly on the atomic configurations included in the calculations. It is still an open question (Peyrusse *et al.*, 2006; Hansen *et al.*, 2007; Chung *et al.*, 2007) which is the most suitable election of them. However, our experience with RAPCAL has led us to consider a "complete" set of configurations, in the sense that the addition of new configurations will not change the results, which allows us to obtain accurate results.

Table 2. *Average ionization for different conditions of temperature and electron density. Results from ATOMIC (Colgan et al., 2006) and RAPCAL codes for configuration average (ATOMIC-DCA, RAPCAL-AP) and detailed level (ATOMIC-DLA, RAPCAL-DLA) accounting approximations*

T(eV)		$N_e(cm^{-3})$ 10^{13}	10^{15}	10^{17}	10^{19}
3	ATOMIC-DCA	1.486	1.895	1.948	0.959
	RAPCAL-AP	1.605	1.786	1.917	1.142
	ATOMIC-DLA	1.730	1.923	1.952	1.004
	RAPCAL-DLA	1.619	1.852	1.913	0.932
5	ATOMIC-DCA	2.055	2.592	2.979	2.104
	RAPCAL-AP	2.057	2.309	2.948	2.182
	ATOMIC-DLA	2.165	2.514	2.976	2.076
	RAPCAL-DLA	2.135	2.276	2.878	2.084
7	ATOMIC-DCA	2.729	3.189	3.718	2.993
	RAPCAL-AP	2.722	3.004	3.529	3.001
	ATOMIC-DLA	2.887	3.185	3.729	2.987
	RAPCAL-DLA	2.873	2.977	3.545	2.998
10	ATOMIC-DCA	3.701	3.856	3.978	3.785
	RAPCAL-AP	3.684	3.747	3.955	3.776
	ATOMIC-DLA	3.723	3.862	3.979	3.786
	RAPCAL-DLA	3.705	3.745	3.956	3.787

https://doi.org/10.1017/S026303460800044X Published online by Cambridge University Press

3.1. Carbon Plasmas

In Table 1, we listed the set of configurations and the number of relativistic configurations and resulting levels considered for the carbon ions. In the table, $(n)^w$ denotes all the possible relativistic configurations that arise from the shell n with w bound electrons.

Since radiative properties depend on the average ionization, we started by checking this magnitude. Thus, in Table 2, we compare the average ionization for low temperatures and moderate densities, which correspond to NLTE situations, calculated using RAPCAL with those provided by Colgan *et al.* (2006) using ATOMIC code, both under DCA (ATOMIC-DCA), and DLA (ATOMIC-DLA) approaches. This code is a detailed kinetics model developed at the Los Alamos National Laboratory (LANL), which includes configuration interaction effects for atomic data as well as quantum mechanical calculation for cross sections of the atomic processes. As we can see there is a general agreement between the RAPCAL and ATOMIC results both in DCA and DLA situations, obtaining relative errors that are in general lower than 5%. This is a remarkable result, since our kinetic model is based on analytical expressions for the cross sections and therefore this reduces considerably the complexity and the computing time. Moreover, it is also observed that RAPCAL-AP also gives acceptable results. This fact has been proved in the Fourth NLTE Kinetics Codes Comparison Workshop (Rubiano *et al.*, 2007). Since the analytical potentials of the atomic module of RAPCAL avoid the iterative procedures of the self-consistent calculations, RAPCAL-AP allow us to make fast computations of plasma average ionization and ion populations.

Taking into account the simplicity of the RAPCAL-PA calculations and its acceptable accuracy, this was used in a previous work (Gil *et al.*, 2008) to obtain maps of the average ionization and the plasma regimes (LTE, NLTE,

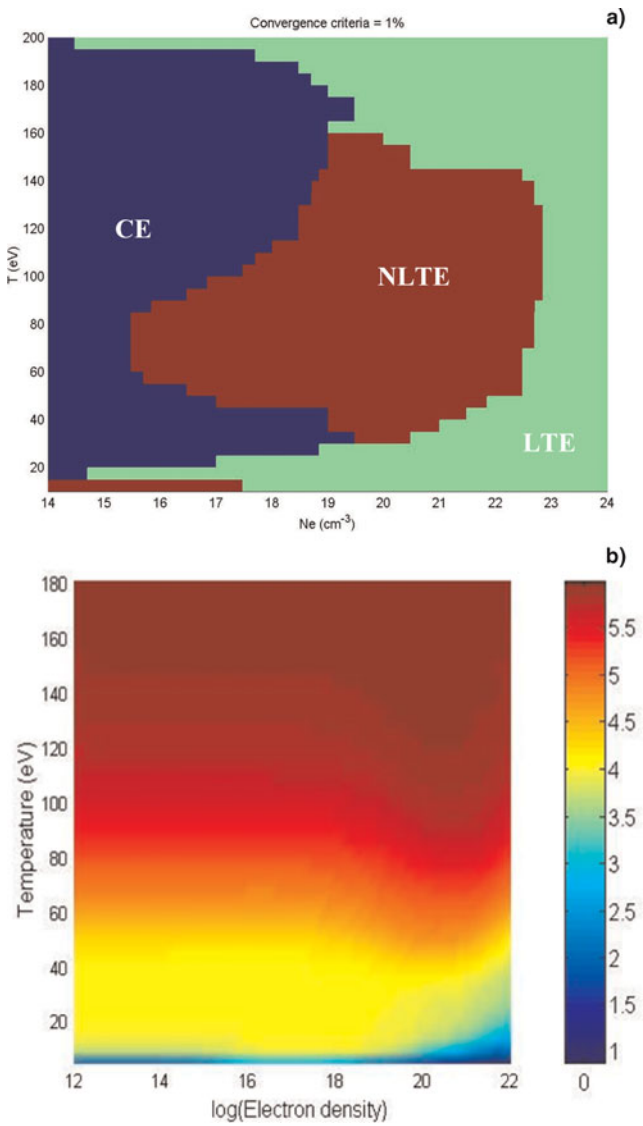

Fig. 1. (Color online) Carbon plasma regimes **(a)** and average ionization **(b)** as a function of electron density and temperature.

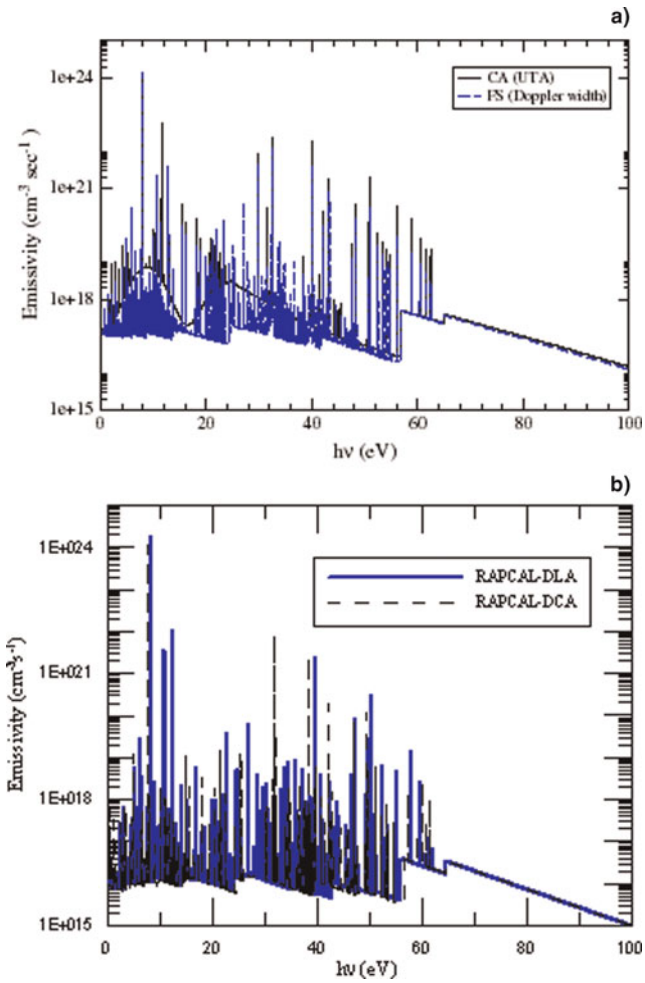

Fig. 2. (Color online) **(a)** Emissivity of carbon at an electron temperature of 10 eV and density of 10^{15} cm^{-3}. **(b)** Comparisons with results from Colgan *et al.* (2006).

https://doi.org/10.1017/S026303460800044X Published online by Cambridge University Press

Table 3. *Rosseland and Planck mean opacities for optically thin carbon plasmas assuming LTE approach. The results are compared with those provided by LEDCOP code (Magee et al., 1995)*

		Planck mean opacity (cm^2/g)		Rosseland mean opacity (cm^2/g)	
T(eV)	ρ (g/cm^3)	RAPCAL	LEDCOP	RAPCAL	LEDCOP
10	10^{-5}	1693	1329	119	163
20		59	63	4	5
10	10^{-3}	46255	51471	17580	18083
20		1780	2366	298	362

and CE) for optically thin carbon plasmas, as a function of electron density and temperature. These maps are illustrated in Figure 1. The map of plasma regimes was elaborated by applying a criterion on the ion populations and it was proved that its predictions agree with those obtained using Griems criterion (Griem, 1963), though our method can state the regime of the whole plasma. This map gives useful *a priori* information for many topics of plasma. Moreover, from the point of view of computational time, it also implies a considerable saving, since the resolution of CE and Saha equations for carbon plasmas only requires to solve 6×6 matrices, whereas the rate equations entail to handle with matrices of very high order because the number of levels (and, therefore, transitions) needed to get accurate results under NLTE conditions is usually very large (in our case, for example, 31928×31928).

In order to check the results of radiative properties we plotted in Figure 2, the spectrally resolved emissivity for given plasma conditions versus the calculations given in Colgan *et al.* (2006). The line profile considered is a Doppler one. As we can see, the emissivities obtained using both codes under DLA approach are very similar, showing the same structures at comparable energy positions. Furthermore, we have also plotted the emissivity calculated using RAPCAL-AP. We can observe that there is a diminution of lines with respect to RAPCAL-DLA calculations and also that some lines are shifted. These results are expected since the DCA approach entails a lower number of transitions and, moreover, the atomic data provided by the atomic module implemented in RAPCAL are not so good than those given by FAC code. This fact produces a shift on the position of the peaks. Therefore, the simple atomic model is able to provide accurate results of atomic magnitudes such as the average ionization and ion populations and due to its simplicity and low computing cost, it is useful to optimize more complex calculations (by means of the maps given in Figs. 1a and 1b, for instance). On the contrary, when very detailed calculations are required, as the spectrally resolved emissivities, the RAPCAL-AP model can only provide qualitatively results and RAPCAL-DLA calculations are required.

Finally, in Table 3, Planck and Rosseland mean opacities for two densities and temperatures are compared with the LTE opacities calculation code LEDCOP (Magee *et al.*, 1995) developed at LANL. This code uses a basis set of detailed LS terms including interactions with the plasma which are treated as perturbations. With the help of Figure 1a we have checked that the LTE assumption is appropriate for all the conditions shown in the table. It is observed to be a good agreement between both results.

3.2. Aluminum Plasmas

In Table 4, are listed the number of configurations and levels considered for the seven first ions of aluminum and the set of configurations selected. For the rest of the ions, they were presented in Table 1. Once more and using RAPCAL-AP calculations, we carried out the same maps for carbon cases which are displayed in Figure 3.

As we did for carbon plasmas, we start analyzing the results obtained with RAPCAL for the average ionization. In this case, we also compared the integer charge state distribution (see Table 5). The plasma conditions are $T = 40$ eV and $\rho = 0.0135\ \mathrm{gcm}^{-3}$, in which we can assume LTE conditions according to Figure 3a. We have performed calculations both with RAPCAL-AP and RAPCAL-DLA. The results are compared with those provided by Zeng and Yuan (2002) that solve the Saha-Boltzmann equations in the DTA approach, including a large number of levels, and Faussurier *et al.* (1997) who proposed a method based on the average atom (AA) model. The first feature that we can observe is the good agreement among the different

Table 4. *Set of configurations and numbers of relativistic configurations and levels considered in the calculations performed by RAPCAL code for the seven first aluminum ions ($n \leq 10$, $n' \leq 6$)*

	Al-like	Mg-like	Na-like	Ne-like	F-like	O-like	N-like
	$(3)^3$	$(3)^2$	$(3)^1$	$(2)^8$	$(2)^7$	$(2)^6$	$(2)^5$
	$(3)^2$nl	$(3)^1$nl	nl	$(2)^7$nl	$(2)^6$nl	$(2)^5$nl	$(2)^4$nl
	$(2)^7(3)^4$	$(2)^7(3)^3$	$(2)^7(3)^2$	$(2)^6(3)^2$	$(2)^5(3)^2$	$(2)^4(3)^2$	$(2)^3(3)^2$
	$(2)^7(3)^3$n'l	$(2)^7(3)^2$n'l	$(2)^7(3)^1$n'l	$(2)^6(3)^1$n'l	$(2)^5(3)^1$n'l	$(2)^4(3)^1$n'l	$(2)^3(3)^1$n'l
Configs	1889	1006	546	1189	1779	2124	2072
Levels	22397	14167	3514	12469	25066	23524	19670

https://doi.org/10.1017/S026303460800044X Published online by Cambridge University Press

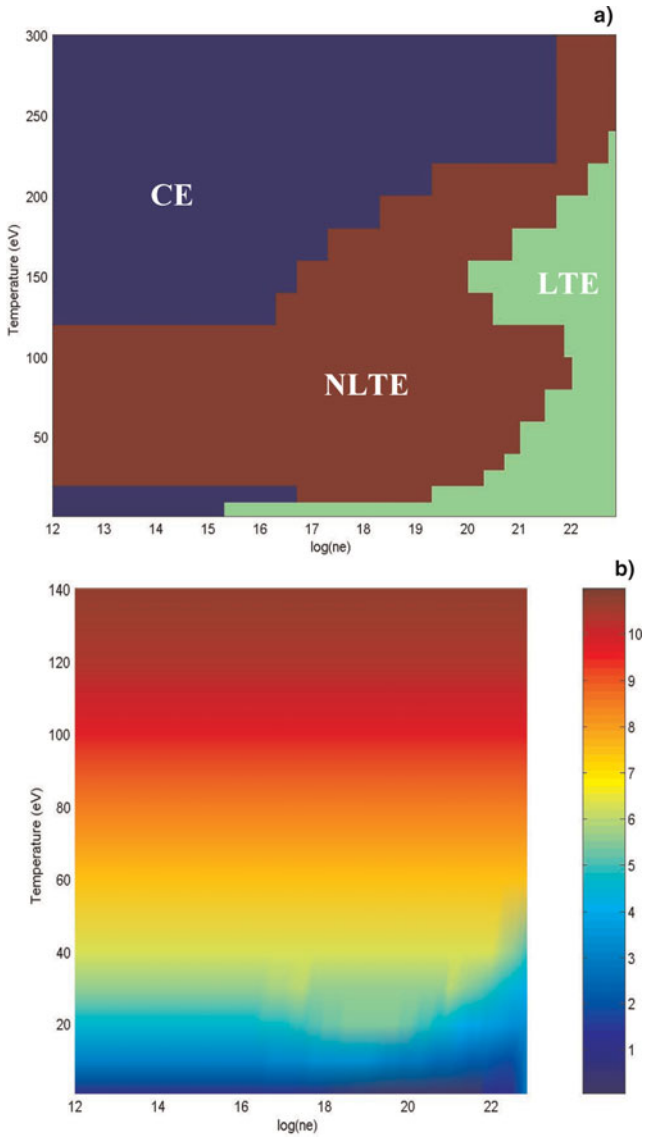

Fig. 3. (Color online) Aluminum plasma regimes (**a**) and average ionization (**b**) as a function of electron density and temperature.

Table 5. *Integer charge state distribution (in percentage) and average ionization ($\bar{Z}$) of an aluminum plasma ($T = 40$ eV, $\rho = 0.0135$ gcm^{-3}) assuming LTE conditions. For comparison our results in DLA approach (RAPCAL-DLA), using the atomic module of RAPCAL (RAPCAL-AP), and those of Zeng and Yuan (2002) and Faussurier et al.* (1997) are given

Charge state	RAPCAL-DLA	RAPCAL-AP	Zeng & Yuan	Faussurier *et al.*
Al^{5+}	4.23	3.54	3.85	2.65
Al^{6+}	25.20	29.71	24.84	22.33
Al^{7+}	44.03	42.90	45.62	46.95
Al^{8+}	23.29	21.06	22.72	24.65
Al^{9+}	3.05	2.57	2.64	3.23
$\bar{Z}$	6.96	6.89	6.95	7.04

calculations for the average ionization, which is excellent between the two detailed calculations. For these calculations it is also found a good accord for the integer charge distributions. The other two models, which are cruder, show shifts toward lower (RAPCAL-DCA) and higher (Faussurier *et al.*, 1997) charge state distributions, although their results are also competitive. This fact is very relevant because these kinds of calculations usually require enormous amounts of computing time and this is considerably reduced when these simple models are used.

As it is known, the plasma transmission is a useful tool for spectroscopic diagnostics of plasma temperature, and since the transmission is related straight to the opacity, its analysis permits to check the opacity models. In particular, we have studied the transmission spectrum of an aluminum plasma experimentally obtained with the iodine laser ASTERIX at the Max-Planck-Institut für Quantenoptik reported by Winhart *et al.* (1995). The plasma conditions were $T \sim 20$ eV and $\rho \sim 0.01$ gcm^{-3}, the spectral range $70 \leq h\nu \leq 280$ eV and the sample layer was 1075 Å. According to that work, LTE is a reasonable assumption for these conditions. Taking into account the average ionization provided, about 4.3, it gives an electron density around 10^{21} cm^{-3} and Figure 3a also corroborates the validity of the assumption. In Figure 4, we present our result calculated under DLA approach compared with the experimental one and the obtained by the widely known opacity code OPAL (Rogers *et al.*, 1992).

From the figure, we can observe that in general our agreement with the experimental data and OPAL results is quite good. This agreement is better both at low and high wavelengths. However, it can be observed that our model predicts a greater transmission, and therefore a lower opacity, in the range 95–105 Å. On the contrary, OPAL seems to reproduce better this region of the spectrum although it overestimates the transmission in the higher range of wavelengths. Some of the differences between both theoretical results can be explained taking into account that the average ionization predicted by OPAL is 4.30 whereas we obtain 4.18. Although they are very similar, discrepancies in the average ionization

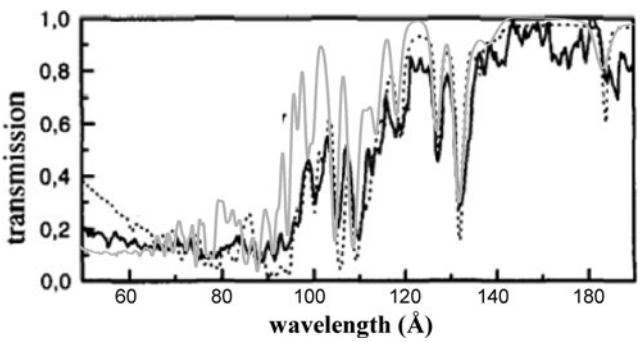

Fig. 4. Comparison of the experimental aluminum transmission spectrum (Winhart *et al.*, 1995) (black solid) with RAPCAL (gray solid) and OPAL (Rogers *et al.*, 1992) (dotted). Plasma conditions are $T = 20$ eV, $\rho = 0.01$ gcm^{-3}.

https://doi.org/10.1017/S026303460800044X Published online by Cambridge University Press

Table 6. *Population of the most abundant ions, average ionization and mean opacities for an aluminum plasma ($T = 20$ eV, $\rho = 0.01$ gcm^{-3}). Comparisons between RAPCAL and results from Zeng et al. (2001) and LEDCOP code (Magee et al., 1995)*

	Population fraction			Average ionization	Mean Opacities (cm^2/g)	
	Al^{3+}	Al^{4+}	Al^{5+}		Rosseland	Planck
Zeng *et al.*	0.16	0.50	0.32	4.20	4184	24891
RAPCAL	0.17	0.49	0.30	4.18	4061	25026
LEDCOP	—	—	—	4.21	4900	24900

imply differences in the ion and level populations which have a dramatically influence in the radiative properties. Zeng *et al.* (2001*b*) also carried out a study of this experiment. They solved the Saha-Boltzmann equations under DTA approach and performed an elaborated calculation of the opacity, obtaining a good agreement with the experiment. In Table 6, we display the population fraction of the most abundant ions obtained by them and using RAPCAL, as well as the average ionization, and the mean opacities, which are also compared with LEDCOP. We can see that our average ionization is very similar to the obtained by the other two calculations and that the population fractions show a good agreement with those reported in Zeng *et al.* (2001*b*). However, our model presents a small shift of the ion population to lower charge states. This confirms that small changes in the average ionization could entail large ones in the level populations and therefore in the radiative properties. From Table 6, it is worth pointing out the excellent agreement among the mean opacities obtained by the three computations.

We also present some calculations of radiative properties under NLTE conditions carried out using RAPCAL-DLA. Thus, in Figures 5 and 6, are displayed the absorption coefficient, and the emissivity for the plasma conditions 400 eV and 0.1778 gcm^{-3} and 160 eV and 0.0056 gcm^{-3}, respectively. The calculations are compared with THERMOS (Nikiforov *et al.*, 1995), which is a widely known opacity code that uses a self-consistent field model with Dirac equations for generating the atomic data and it calculates the NLTE opacities by numerical solution of the rate equations following an improved AA approximation, and DESNA code (Nikiforov *et al.*, 2000) which is a detailed CRSS level-by-level kinetics model that also calculates NLTE emissivities and opacities.

The first thing that we can observe from both figures is that THERMOS results show a lesser line structure than the other two. This fact is expected since, as it was said above, the rate equations in this code are solved in the AA approximation. On the other hand, our results and those of DESNA models show a general agreement with respect to the structure of lines and their positions in the photon energy scale. However, some differences in the number of lines and their intensity are observed, which could obey the fact that in DESNA the detailed structure of ion level configurations is taken into account in LS-link approximation subject to splitting into terms whereas in our case FAC works in the DLA approximation, obtaining the atomic energies by diagonalizing the relativistic Hamiltonian.

3.3. Krypton Plasmas

For the case of krypton, we have analyzed the radiative power loss in the optically thin limit. As it is known, this magnitude is of importance for high-Z plasmas since it allows us to know the radiation emitted and krypton plasmas are employed in multiple applications, where the plasmas range electron temperatures of a few eV to a few keV and electron densities from 10^{14} to 10^{23} cm^{-3}. In the first place, we studied the radiative power loss for low-electron-density ($\leq 2 \times 10^{14}$ cm^{-3})

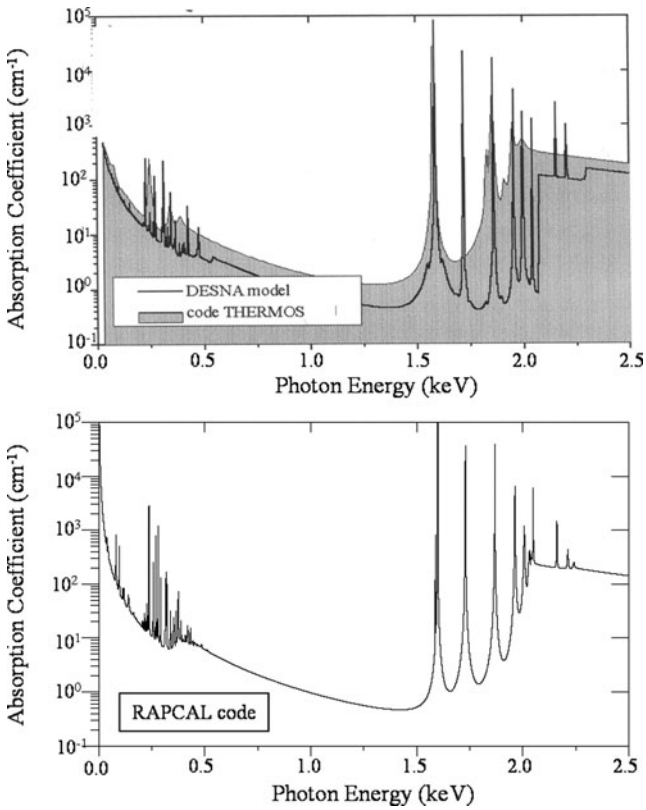

Fig. 5. Absorption coefficient for aluminum plasma under NLTE situation at 400 eV and 0.1778 gcm^{-3}. Comparison of RAPCAL code with THERMOS (Nikiforov *et al.*, 1995) and DESNA (Nikiforov *et al.*, 2000) models.

https://doi.org/10.1017/S026303460800044X Published online by Cambridge University Press

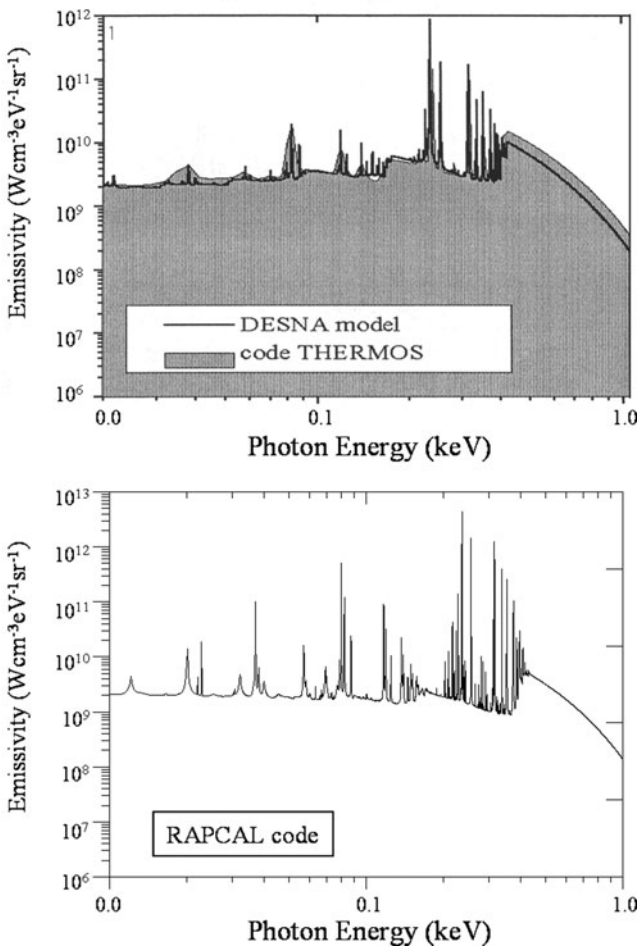

Fig. 6. Emissivity for aluminum plasma under NLTE situation at 160 eV and 0.0056 gcm^{-3}. Comparison of RAPCAL code with THERMOS (Nikiforov *et al.*, 1995) and DESNA (Nikiforov *et al.*, 2000) models.

krypton plasmas for a wide range of temperatures. Our calculations were performed using the atomic module of RAPCAL under relativistic DCA approach (i.e., RAPCAL-AP) and the results are listed in Table 7. They are compared with those obtained using the analytical expression, valid for low density regime only, proposed by Fournier *et al.* (2000). This expression was fitted to total radiative cooling coefficients computed by them and validated with krypton cooling rates derived from tokamak experiments. From the table, we can observe that both results are in general quite similar. Obviously, there are discrepancies but they are small and derive from the differences in the atomic models employed. In these low density situations, the corona equilibrium can be assumed. Under this regime, the plasma average ionization and level populations are almost independent of the density and, therefore, the radiative cooling coefficient does not change. In Table 7, the results shown are obtained as the total radiative cooling coefficient multiplied by the electron and ion densities, i.e., by $n_e^2/\bar{Z}$. For this reason, the dependence of the radiative power loss in Table 7 with the density is only on n_e^2, increasing two orders of magnitude when the density increases one. However, we can observe for the highest density and the two lowest temperatures shown, that our results exhibit a different behavior. This fact implies that for these temperatures, the CE assumption is not accurate enough. Obviously, the calculation performed using the analytical fit does not present this discrepancy since it does not depend on the density.

We have also carried out an analysis for higher density and temperatures. In Table 8, we present the cases considered and the average ionization obtained for those cases. The calculations were made using RAPCAL-AP. The results are compared with those reported by Chung *et al.* (2006). In that work, the calculations performed were very sophisticated. The atomic data were generated by the HULLAC suite of codes (Bar-Shalom *et al.*, 2001). For atomic structure data HULLAC calculates the multi-configuration, intermediate coupling energy eigenvalues of the fine structure levels, and configuration interaction is taken into account for energy level calculations and oscillator strengths (Klapisch, 1971). Autoionization rates (Oreg *et al.*, 1991) and photoionization cross sections were computed using the multiconfiguration wave functions and the collisional excitation and ionization were obtained in the distorted wave approximation (Bar-Shalom *et al.*, 1988). A good agreement between our results and those provided by Chung *et al.* (2006) is found, which is a remarkable fact since, as it was

Table 7. *Radiative power loss (ergs/s/cm^3) for low densities and several temperatures. Comparison between RAPCAL results and those obtained using the fit provided by Fournier et al. (2000)*

	Ne = 10^{12} cm^{-3}		Ne = 10^{13} cm^{-3}		Ne = 10^{14} cm^{-3}	
T (eV)	RAPCAL	Fournier *et al.*	RAPCAL	Fournier *et al.*	RAPCAL	Fournier *et al.*
10	5.600×10^5	2.381×10^5	5.599×10^7	2.382×10^7	3.573×10^9	2.359×10^9
20	3.220×10^5	1.387×10^5	3.217×10^7	1.387×10^7	1.416×10^9	1.387×10^9
50	3.124×10^4	3.467×10^4	3.124×10^6	3.467×10^6	3.123×10^8	3.467×10^8
100	3.522×10^4	7.154×10^4	3.522×10^6	7.154×10^6	3.522×10^8	7.154×10^8
200	9.155×10^4	1.011×10^5	9.155×10^6	1.011×10^7	9.155×10^8	1.011×10^9
500	1.949×10^4	6.331×10^4	1.949×10^6	6.331×10^6	1.949×10^8	6.331×10^8
1000	1.854×10^4	2.726×10^4	1.854×10^6	2.726×10^6	1.854×10^8	2.726×10^8

https://doi.org/10.1017/S026303460800044X Published online by Cambridge University Press

Table 8. *Average charge state of krypton ions. Our results are compared with those given by Chung et al. (2006)*

Ne (cm^{-3})	10^{14}		10^{18}		10^{22}	
T (eV)	RAPCAL	Chung *et al.*	RAPCAL	Chung *et al.*	RAPCAL	Chung *et al.*
1000	25.33	25.48	25.36	25.56	26.69	27.46
1600	26.16	26.64	26.15	26.68	28.65	29.49
2000	26.86	27.82	26.87	27.86	30.16	30.81
2500	28.07	29.70	28.06	29.72	31.65	31.95
3000	30.48	31.24	30.48	31.24	32.51	32.61
3500	31.74	32.12	31.75	32.13	32.97	32.98
4000	32.46	32.65	32.47	32.65	33.22	33.21
4500	32.87	32.96	32.88	32.97	33.38	33.36
5000	33.12	33.17	33.13	33.18	33.49	33.47
6000	33.40	33.42	33.40	33.43	33.61	33.62
7000	33.57	33.58	33.57	33.58	33.71	33.72
8000	33.68	33.69	33.68	33.69	33.79	33.80
10000	33.86	33.84	33.86	33.84	33.93	33.92

stated before, their calculations are very complex. We can observe that for the two lowest densities and for all the temperatures considered, the plasma average ionization is density independent. This fact implies that in these cases the krypton plasma can be assumed under CE conditions. Hence, the total radiative cooling coefficients scaled by the electron densities for these plasma conditions are quite similar, as it is displayed in Figure 7. On the other hand, for the highest temperature considered, the CE approach could be assumed for temperatures higher than 7 keV, as we can see both form Table 8 and Figure 7. Finally, we would like to point out that results displayed in Figure 7 are very similar, both qualitatively and quantitatively, to those reported by Chung *et al.* (2006). As a conclusion, we have obtained that the simple atomic model implemented in RAPCAL can be used to compute radiative power losses and cooling coefficients for high Z elements in a wide range of plasma conditions with reasonable accuracy. This is remarkable result since, as it was said previously, these magnitudes are essential in many topics of the plasma research.

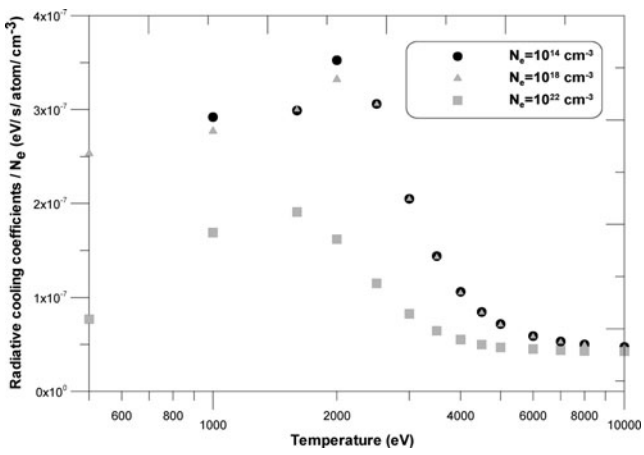

Fig. 7. Total radiative cooling rates scaled by electron density at electron densities of 10^{14} cm^{-3}, 10^{18} cm^{-3} and 10^{22} cm^{-3}.

3.4. Xenon Plasmas

In this last section, we present a simulation of the intensity spectrum of an optically thick xenon plasma obtained by the experiment carried out by Chenais-Popovics *et al.* (2002) at the Laboratoire pour l'Utilisasion des Laseres Intenses (LULI). From the experiment they determined that the plasma was under stationary situation during the laser pulse, where the ion density is 4.75×10^{18} cm^{-3}. The electron temperature, average ionization and electron densities were obtained by fitting simultaneously the electron and ion Thomson scattering spectra and they are, respectively, 415 ± 40 eV, 27.4 ± 1.5, and $1.30 \pm 0.05 \times 10^{20}$ cm^{-3}.

Our calculation was performed assuming an homogeneous plasma with planar symmetry. The calculations were done under relativistic DCA-UTA approach (Bauche-Arnoult *et al.*, 1985) using FAC code and including corrections to the oscillator strengths due to CI. The configurations included in our simulation for xenon ions involved are listed in Table 9. Furthermore, we also include in the table the number of relativistic configurations and line transitions. According to the experimental description, a spectral resolution of 50 mÅ was fixed and the reabsorption effect was introduced assuming a 160 μm path length by means of the escape factor formalism. The simulation was carried out at 450 eV, the upper limit of the estimated error bar in the Thomson scattering measurements, since the agreement obtained for the average ionization at 450 eV is better than for 415 eV. This also happens with the simulation of AVERROES/TRANSPEC, a sophisticated collisional-radiative super-configuration code (Peyrusse, 2000). Thus, the average ionization obtained for this temperature by RAPCAL is 27.1 whereas AVERROES gives 26.8 (Chenais-Popovics *et al.*, 2002). Both of them are in agreement with the Thomson scattering results. In Figure 8, we present the

https://doi.org/10.1017/S026303460800044X Published online by Cambridge University Press

Table 9. *Set of configurations selected and number of relativistic configurations and line transitions included in the calculations performed by RAPCAL code for the xenon ions involved ($n \leq 8$, $n' \leq 5$, $n'' \leq 6$)*

	Ge-like	Ga-like	Zn-like	Cu-like	Ni-like
	$(4)^4$	$(4)^3$	$(4)^2$	$(4)^1$	$(3)^{18}$
	$(4)^3$nl	$(4)^2$nl	$(4)^1$nl	$(3)^{18}$nl	$(3)^{17}$nl
	$(4)^2(5)^2$	$(4)^1(5)^2$	$(5)^2$	$(3)^{17}(4)^2$	$(3)^{16}(4)^2$
	$(4)^2(5)^1(6)^1$	$(4)^1(5)^1(6)^1$	$(5)^1(6)^1$	$(3)^{17}(4)^1$n'',^{1}	$(3)^{16}(4)^1$n'',^{1}
	$(4)^2(6)^2$	$(4)(6)^2$	$(6)^2$		
	$(3d)^9(4)^5$	$(3d)^9(4)^4$	$(3)^{17}(4)^3$		
	$(3d)^9(4)^4$n'l	$(3d)^9(4)^3$nl	$(3)^{17}(4)^2$n'l		
Configs	6596	2529	1581	651	1240
Lines	55498	18564	10633	4237	8848
	Co-like	Fe-like	Mn-like	Cr-like	V-like
	$(3)^{17}$	$(3)^{16}$	$(3)^{15}$	$(3)^{14}$	$(3)^{13}$
	$(3)^{16}$nl	$(3)^{15}$nl	$(3)^{14}$nl	$(3)^{13}$nl	$(3)^{12}$nl
	$(3)^{15}(4)^2$	$(3)^{14}(4)^2$	$(3)^{13}(4)^2$	$(3)^{12}(4)^2$	$(3)^{11}(4)^2$
	$(3)^{15}(4)^1$n''l	$(3)^{14}(4)^1$n''l	$(3)^{13}(4)^1$n''l	$(3)^{12}(4)^1$n''l	$(3)^{11}(4)^1$n''l
Configs	1958	2418	2881	3050	2819
Lines	14328	19931	24561	10663	26167

intensity spectrum obtained using RAPCAL compared with the experimental one (Chenais-Popovics *et al.*, 2002) and the one provided by ATOMIC (Fontes *et al.*, 2006). The latter calculation was carried out with the relativistic UTA formalism, and therefore, it is comparable to RAPCAL results. The main features of the experimental spectrum appear in the region of wavelengths larger than 12.5 Å associated to the 3d−4f transition array. The higher peaks are related to Co-like and Fe-like ions. In the spectrum calculated by RAPCAL they are also the main ones although the relation between the intensities

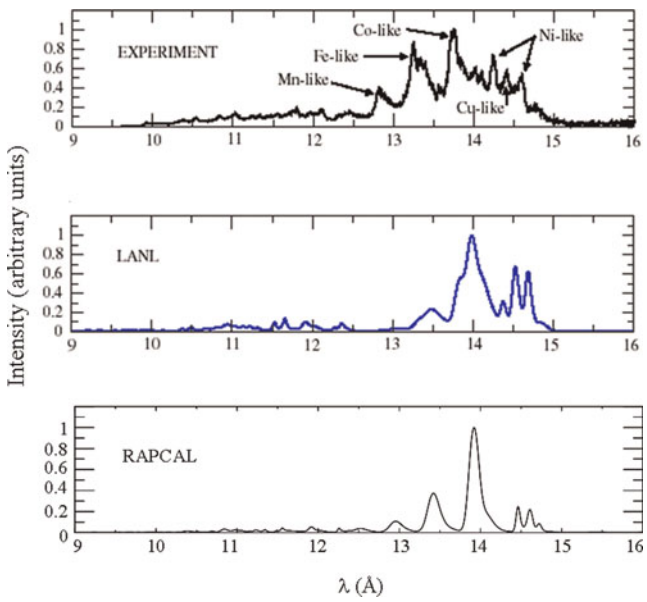

Fig. 8. (Color online) Experimental, ATOMIC and RAPCAL xenon intensity data. The numerical calculations were performed assuming $T = 450$ eV and $n_i = 4.75 \times 10^{18}$ cm^{-3}.

of the peaks disagrees with the experimental situation. This fact is due to our calculations under-populate the Fe-like ion. On the other hand, in the spectrum provided by ATOMIC the transitions associated to Ni-like and Cu-like ions are larger than the Fe-like and the peak linked to the transition array of the Mn-like ion is not present. This one appears in the RAPCAL calculation but our code underestimates the populations of Ni and Cu-like ions. It seems like the ATOMIC code provides a lower ionization than the RAPCAL code. In Fontes *et al.* (2006), the authors considered the possibility that some differences between the theoretical and experimental spectra could come from the fact that the temperature might be higher than the one experimentally measured. However, their calculations at temperatures of 500 and 600 eV improve the range of lower wavelengths but increase the discrepancies in the opposite range of wavelengths. We would like to point out that the experimental spectrum is a time-integrated one and, therefore, it could occur that we were not able to fit the whole spectrum under the assumption of uniform plasma.

Another source of discrepancy is the spectral detail of the calculation. In order to obtain better results, a DLA description including full CI is required. However, a detailed level calculation for an ion as complex as xenon would include a huge amount of levels and transitions and the problem would become intractable. Therefore, hybrid models that combine DLA description including CI for the most relevant levels and transitions and other approaches for the rest seem to be the solution. In particular, in Fontes *et al.* (2006), a calculation is performed of the xenon spectra making use of an hybrid model based on the "dual method" described in Abadallah *et al.* (2001) and the spectrum obtained presents a better agreement with the experimental data than in the DCA-UTA calculation. Therefore, taking into account that the RAPCAL DCA-UTA calculation provides an accurate

https://doi.org/10.1017/S026303460800044X Published online by Cambridge University Press

value for the average ionization and an estimation of the spectra similar to the ATOMIC DCA-UTA, it is also expected that an hybrid model can improve our results dramatically. $T = 450$ eV and $n_i = 4.75 \times 10^{18}$ cm^{-3}.

4. CONCLUSIONS

A new flexible code to obtain accurate optical properties for optically thin and thick plasmas in a wide range of densities and temperatures has been presented. In this code, the level populations are obtained solving a CRSS model which employs analytical expressions for the rate coefficients of the atomic processes, which yield a substantial saving of computational requirements but providing satisfactory results as it has been shown. It used the matrix sparse technique for the storage, which allow us to include a large number of atomic levels, and iterative procedures in order to accelerate the resolution of the set of equations. The self-absorption effects in homogeneous plasmas are modeled using the escape factor formalism for planar, cylindrical, and spherical symmetries. The atomic data required can be provided to the code both as an input file or they can be generated using the atomic module implemented in RAPCAL, which is based on analytical potentials under the relativistic DCA approach. This last option is very useful when we are interested in providing radiative properties to simulations that require opacities and emissivities to hydro-codes and, therefore, celerity is desired although some accuracy is lost.

We have presented results for ion populations, plasma average ionization, spectrally resolved opacities and emissivities, mean opacities, transmission and intensity spectrum, and radiative power loss. We have considered low-, medium- and high-Z elements (C, Al, Kr, and Xe), both in LTE and NLTE situations, in a wide range of plasma conditions. Furthermore, we have analyzed the opacity effects in the ion populations and the intensity spectrum in an optically thick homogeneous plasma. We have performed calculations using both very accurate atomic data provided by FAC code and using the simple model implemented in RAPCAL. For all the calculations shown, we have made comparisons with experimental data or with theoretical ones provided by well known numerical codes. We have obtained that the simple atomic model based in analytical potentials implemented in RAPCAL is useful and accurate in order to compute ion populations, plasma average ionization or radiative power losses and also to optimize more detailed and complex calculations by means of the maps of the average ionization and plasma regimes presented. However, for magnitudes such as spectrally resolved opacities and emissivities, this simple model is not accurate enough and it only gives qualitatively conclusions. On the other hand, the calculations made using RAPCAL with atomic data from FAC show good agreements for all the magnitudes analyzed.

In this work, we have presented calculations using the atomic module of RAPCAL using as effective potential the isolated analytical one. However, as it was said previously, we have also developed analytical potentials that model strongly and weakly coupled plasmas. It is our purpose in a future work to carry out calculations of radiative properties using these potentials.

Finally, there are two tasks that need to be considered. The first one is the development of a hybrid model that allows us to handle high Z elements with more precision, mixing DLA approach for the ions which has more influence on the spectrum and DCA approach for the others. The second one is to extend the opacity effects to non-homogeneous plasmas.

ACKNOWLEDGMENTS

This work has been supported by a Research Project of the Spanish Science and Education Ministry and also by the "Keep in touch" Project of the European Union.

REFERENCES

Abadallah, J. Jr., Batani, D., Desai, T. Lucchini, G., Faenov, A., Pikuz, T., Magunov, A. & Narayanan, V. (2007*b*). High resolution X-ray emission spectra from picosecond laser irradiated Ge targets. *Laser Part. Beams* **25,** 245–252.

Abdallah, J. Jr., Kilcrease, D.P., Magee, N.H., Mazevet, S., Hakel, P. & Sherrill, M. (2007*a*). Spectral line strength binning method for opacity calculations. *High Energy Density Phys.* **3**, 309–313.

Abdallah, J. Jr., Zhang, H.L., Fontes, C.J., Kilcrease, D.P. & Archer, B.J. (2001). Model comparisons for high-Z non-LTE steady-state calculations. *J. Quant. Spectrosc. Radiat. Trans.* **71**, 107–116.

Alexiou, S., Calisti, A., Gauthier, P., Klein, L., Leboucher-Dalimier, E., Lee, R.W., Stamm, R. & Talin, B. (1997). Aspects of plasma spectroscopy: recent advances. *J. Quant. Spectrosc. Radiat. Trans.* **58**, 399–413.

Bar-Shalom, A., Klapisc, H.M. & Oreg, J. (2001). HULLAC, an integrated computer package for atomic processes in plasmas. *J. Quant. Spectrosc. Radiat. Trans.* **71**, 169–188.

Bar-Shalom, A., Klapisch, M. & Oreg, J. (1988). Electron collision excitations in complex spectra of ionized heavy atoms. *Phys. Rev. A.* **38**, 1773–1784.

Bar-Shalom, A., Oreg, J. & Klapisch, M. (1997). Non-LTE superconfiguration collisional radiative model. *J. Quant. Spectrosc. Radiat. Trans.* **58**, 427–439.

Bar-Shalom, A., Oreg, J., Goldstein, W.H., Shvarts, D. & Zigler, A. (1989). Super-transition-arrays: A model for the spectral analysis of hot dense plasmas. *Phys. Rev. A.* **40**, 3183–3193.

Bauche, J., Bauche-Arnoult, C. & Klapisch, M. (1987). Transition arrays in the spectra of ionized ions. *Adv. At. Mol. Phys.* **23**, 131–195.

Bauche, J., Bauche-Arnoult, C. & Peyrusse, O. (2006). Effective temperatures in hot dense plasmas. *J. Quant. Spectrosc. Radiat. Trans.* **99**, 55–66.

Bauche-Arnoult, C., Bauche, J. & Klapisch, M. (1985). Variance of the distributions of energy levels and of the transition arrays in atomic spectra. III. Case of spin-orbit-split arrays. *Phys. Rev. A* **31**, 2248–2259.

https://doi.org/10.1017/S026303460800044X Published online by Cambridge University Press

Bowen, C. (2001). NLTE emissivities via ionisation temperature. *J. Quant. Spectrosc. Radiat. Trans.* **71**, 201–214.

Bowen, C., Decoster, A., Fontes, C.J., Fournier, K.B., Peyrusse, O. & Ralchenko, Yv. (2003). Review of the NLTE emissivities code comparison virtual workshop. *J. Quant. Spectrosc. Radiat. Trans.* **81**, 71–84.

Bowen, C., Lee, R.W. & Ralchenko, Y. (2006). Comparing plasma population kinetics codes: Review of the NLTE-3 Kinetics Workshop. *J. Quant. Spectrosc. Radiat, Trans.* **99**, 102–119.

Chenais-Popovics, C., Malka, V., Gauthier, J.C., Gary, S., Peyrusse, O., Rabec-Le Gloahec, M., Matsushima, I., Bauche-Arnoult, C., Bachelier, A. & Bauche, J. (2002). X-ray emission of a xenon gas jet plasma diagnosed with Thomson scattering. *Phys. Rev. E.* **65,** 0464181.

Chung, H.K., Chen, M.H. & Lee, R.W. (2007). Extension of atomic configuration sets of the non-LTE model in the application to the Kα diagnostics of hot dense matter. *High Energy Density Phys.* **3**, 57–64.

Chung, H.K., Chen, M.H., Morgan, W.L., Ralchenko, Y. & Lee, R.W. (2005). FLYCHK: Generalized population kinetics and spectral model for rapid spectroscopic analysis for all elements. *High Energy Density Phys.* **1**, 3–12.

Chung, H.K., Fournier, K.B. & Lee, R.W. (2006). Non-LTE kinetics modelling of krypton ions: Calculation of radiative cooling coefficients. *High Energy Density Phys.* **2**, 7–15.

Colgan, J., Fontes, C.J. & Abdallah, J. Jr. (2006). Collisional-radiative studies of carbon plasmas. *High Energy Density Phys.* **2**, 90–96.

Cowan, R.D. (1981). *The Theory of Ttomic Structure*. Berkeley, CA: University of California Press.

Csanak, G. & Daughton, W. (2004). The application of the single-channel random phase approximation to radiative properties of dense He and Li plasmas. *J. Quant. Spectrosc. Radiat. Trans.* **83**, 83–92.

Dimitrijevic, M.S, & Konjevic, N. (1980). Stark widths of doubly-ionized and triply-ionized atom lines. *J. Quant. Spectrosc. Radiat. Trans.* **24**, 451–459.

Dimitrijevic, M.S., Konjevic, N. (1987). Simple estimates for Stark-broadening of ion lines in stellar plasmas. *Astron. Astrophys.* **172**, 345–349.

Faussurier, G., Blancard, C. & Decoster, A. (1997). Statistical mechanics of highly charged ions in local thermodynamic equilibrium. *Phys. Rev. E.* **56**, 3474–3487.

Filevich, J., Grava, J., Purvis, M., Marconi, M.C., Rocca, J.J., Nilsen, J., Dunn, J. & Johnson, W.R. (2007). Multiply ionized carbon plasmas with index of refraction greater than one. *Laser Part. Beams.* **25**, 47–51.

Florido, R. (2007). ABAKO. *Un modelo para el estudio de la cinética de poblaciones y propiedades radiativas de plasmas bajo condiciones de no-equilibrio (A model for the study of population kinetics and radiative properties of plasmas under non-equilibrium conditions)*. PhD Thesis. Las Palmas: Gran Canaria: University of Las Palmas de Gran Canaria.

Florido, R., Gil, J.M., Rodriguez, R., Rubiano, J.G., Martel, P. & Mínguez, E. (2005). Using sparse matrices techniques and iterative solver in the calculation of level populations for NLTE plasmas. *EPS Plasma Phys.* **29C**, P-5.124.

Florido, R., Gil, J.M., Rodriguez, R., Rubiano, J.G., Martel, P. & Minguez, E. (2006). Line photon transport in a non-homogeneous plasma using coupling coefficients. *J. Phys. IV.* **133**, 993–996.

Florido, R., Rodriguez, R., Gil, J.M., Rubiano, J.G., Martel, P., Suárez, D., Mendoza, M. & Mínguez, E. (2008). ABAKO: A new code for population kinetics and radiative properties of plasmas under NLTE conditions. *J. Phys.* **112**, 04208.

Fontes, C.J., Colgan, J., Zhang, H.L. & Abdallah, J. Jr. (2006). Large-scale kinetics modelling of non-LTE plasmas. *J. Quant. Spectrosc. Radia.t Trans.* **99**, 175–185.

Fournier, K.B., May, M.J., Pacella, D., Finkenthel, M., Gregory, B.C. & Goldstein, W.H. (2000). Calculation of the radiative cooling coefficient for krypton in a low density plasma. *Nucl. Fusion.* **40**, 847–863.

Gil, J.M., Martel, P., Minguez, E., Rubiano, J.G., Rodríguez, R. & Ruano, F.H. (2002). An effective analytical potential including plasma effects. *J. Quant. Spectrosc. Radiat. Trans.* **75**, 539–557.

Gil, J.M., Rodriguez, R., Florido, R., Rubiano, J.G., Martel, P. & Minguez, E. (2008). Determination of corona, LTE and NLTE regimes of optically thin carbon plasmas. *Laser Part. Beams* **26**, 21–31.

Griem, H.R. (1963). Validity of local thermodynamic equilibrium in plasma spectroscopy. *Phys. Rev.* **131**, 1170–1176.

Griem, H.R. (1974). *Spectra Line Broadening*. New York: New York Academic.

Griem, H.R. (1997). *Principles of Plasma Spectroscopy*. Cambridge, UK: Cambridge University Press.

Gu, M.F. (2003). Indirect X-ray line-formation processes in iron L-shell ions. *Astrophys. J.* **582**, 1241–1250.

Hakel, P., Sherrill, M.E., Mazevet, S., Abdallah, J. Jr., Colgan, J., Kilkrease, D.P., Magee, N.H., Fontes, C.J. & Zhang, H.L. (2006). The new Los Alamos opacity code ATOMIC. *J. Quant. Spectrosc. Radiat. Trans.* **99**, 265–271.

Hansen, S.B., Bauche, J., Bauche-Arnoult, C. & Gu, M.F. (2007). Hybrid atomic models for spectroscopic plasma diagnostics. *High Energy Dens. Phys.* **3**, 109–114.

Iglesias, C.A., Chen, M.H., Sonnad, V. & Wilson, B.G. (2003). A new detailed accounting opacity code for mid-Z elements: TOPAZ. *J. Quant. Spectrosc. Radiat. Trans.* **81**, 227–236.

Karzas, W.J. & Latter, R. (1961). Electron radiative transitions in a Coulomb field. *Astrophys J.* **6**, 167–212.

Keskinen, M.J. & Schmitt, A. (2007). Non-local heat flow in high-Z laser plasmas with radiation transport. *Laser Part. Beams* **25**, 333–337.

Klapisch, M. (1971). A program for atomic wavefunction computations by the parametric potential method. *Comput. Phys. Commun.* **2**, 239–260.

Kohn, W. & Sham, L.J. (1965). Self-consistent equations including exchange and correlations effects. *Phys. Rev. A.* **140**, 1133–1965.

Kramers, H.A. (1923). On the theory of X-ray absorption and of the continuous X-ray spectrum. *Philos. Mag.* **46**, 836–871.

Liberman, D.A., Cromer, D.T. & Weber, J.T. (1971). Relativistic self-consistent field program for atoms and ions. *Comput. Phys. Commun.* **2**, 107–113.

Lomonosov, I.V. (2007). Multi-phase equation of state for aluminium. *Laser Part. Beams* **25**, 567–84.

Lotz, W. (1968). Electron-impact ionization cross sections and ionization coefficients for atoms and ions from hydrogen to calcium. *Z. Phys.* **216**, 241–247.

Magee, N.H., Abdallah, J. Jr. & Clark, R.E.H. (1995). Atomic structure calculations and new Los Alamos astrophysical opacities. *Astron. Astrophys.* **78**, 51–56.

Mancini, R.C., Joyce, R.F. & Hooper, C.F. (1987). Escape factors for Stark-broadened line-profiles. *J. Phys. B: At. Mol. Phys.* **20**, 2975–2987.

Mandrekas, J., Stacey, W.M. & Kelly, F. (1996). Impurity seeded radiative power exhaust solutions for ITER. *Nucl. Fusion.* **36**, 917–926.

Martel, P., Doreste, L., Mínguez, E. & Gil, J.M. (1995). A parametric potential for ions from helium to iron isoelectronic sequences. *J. Quant. Spectrosc. Radiat. Trans.* **54**, 621–636.

Martel, P., Rubiano, J.G., Gil, J.M, Doreste, L. & Minguez, E. (1998). Analytical expressions for the n-order momenta of charge distribution for ions. *J. Quant. Spectrosc. Radiat. Trans.* **60**, 623–633.

Mazevet, S. & Abdallah, J. Jr. (2006). Mixed UTA and detailed treatment for mid-Z opacity and spectral calculations. *J. Phys. B: At. Mol. Phys.* **39**, 3419–3429.

Mihalas, D. (1978). *Stellar Atmospheres*. San Francisco: Freeman.

Mínguez, E. (1993). *Radiation transport in ICF targets*. In *Nuclear Fusion by Inertial Confinement: A Comprehensive Treatise* (Velarde, G., Ronen, Y. & Martínez-Val, J.M., eds), pp. 198–209. Boca Raton, FL: CRC Press.

Mínguez, E., Gil, J.M., Martel, P., Rubiano, J.G., Rodriguez, R. & Doreste, L. (1998). Developments and comparison of two DENIM opacity models. *Nuc.l Instr. Meth. Phys. Res. A* **415**, 539–542.

Mínguez, E., Rodriguez, R., Gil, J.M., Sauvan, P., Florido, R., Rubiano, J.G., Martel, P. & Mancini, R. (2005). Opacities and line transfer in high density plasma. *Laser Part. Beams* **23**, 199–203.

Nikiforov, A.F., Novikov, V.G. & Uvarov, V.B. (2000). *Quantum-Statistical Models of Hot Dense Matter And Methods for Computation Opacity fnd Equation of State*. Moscow: Fizmattlit.

Nikiforov, A.F., Novikov, V.G., Uvarov, V.B., Dragalov, V.V. & Solomyannaya, A.D. (1995). THERMOS opacity code. *Proc. Third International Opacity Workshop Code Comparison Study*. Garching, Germany: Max-Planck Institute for Quantenoptik.

Oreg, J., Goldstein, W.H. & Klapisch, M. (1991). Autoinization and radiationless electron capture in complex spectra. *Phys. Rev. A.* **44**, 1750–1758.

Orlov, N.Y., Gus'kov, S.Y., Pikuz, S.A., Rozanov, V.B., Shelkovenko, T.A., Zmitrenko, N.V. & Hammer, D.A. (2007). Theoretical and experimental studies of the radiative properties of hot dense matter for optimizing soft X-ray sources. *Laser Part. Beams* **25**, 415–23.

Peyrusse, O. (2000). A superconfiguration model for broadband spectroscopy of non-LTE plasmas. *J. Phys. B: At. Mol. Phys.* **33**, 4303–4322.

Peyrusse, O. (2001). On the superconfiguration approach to model NLTE plasma emission. *J. Quant. Spectrosc. Radiat. Trans.* **71**, 571–579.

Peyrusse, O. (2004). Complex atom physics and radiative properties of hot dense plasmas. *Nucl. Fusion.* **44**, S202–207.

Peyrusse, O., Bauche-Arnoult, C. & Bauche, J. (2006). Effective superconfiguration temperature and the radiative properties of nonlocal thermodynamical equilibrium hot dense plasma. *Phys. Plasmas.* **12**, 0633021.

Post, D.E. (1995). A review of recent developments in atomic processes for divertors and edge plasmas. *J. Nucl. Mater.* **222**, 143–157.

Rajagopal, A.K. (1980). Theory of inhomogeneous electron systems: Spin-density-functional formalism. *Advan. Chem. Phys.* **41**, 59–193.

Rodriguez, R., Gil, J.M. & Florido, R. (2007). Screening effects on the atomic magnitudes of non-hydrogenic ions in strongly coupled plasmas. *Phys. Scr.* **76**, 418–427.

Rodriguez, R., Gil, J.M., Florido, R, Rubiano, J.G., Martel, P. & Mínguez, E. (2006). Code to calculate optical properties for plasmas in a wide range of densities. *J. Phys. IV* **133**, 981–984.

Rodriguez, R., Rubiano, J.G., Gil, J.M., Martel, P., Mínguez, E. & Florido, R. (2002). Development of an analytical potential to include excited ions. *J. Quant. Spectrosc. Radiat. Trans.* **75**, 723–739.

Rogers, F.J., Iglesias, C.A. & Wilson, B.G. (1992). Radiative atomic Rosseland mean opacity tables. *Astrophys. J. Suppl. Ser.* **79**, 507–568.

Rose, S.J. (1992). Calculation of the radiative opacity of laser-produced plasma. *J. Phys. B: At. Mol. Opt. Phys.* **25**, 1667–1681.

Rubiano, J.G., Florido, R., Bowen, C., Lee, R.W. & Ralchenko., Y. (2007). Review of the 4th NLTE code comparison workshop. *High Energy Density Phys.* **3**, 225–232.

Rubiano, J.G., Florido, R., Rodriguez, R., Gil, J.M., Martel, P. & Mínguez, E. (2004). Calculation of the radiative opacity of laser-produced plasmas using a new relativistic-screened hydrogenic model. *J. Quant. Spectrosc. Radiat. Trans.* **83**, 159–182.

Rutten, R.J. (1995). *Radiative transfer in stellar atmospheres*. Sterrekundig Instituut: Utretch.

Seaton, M.J. (1990). Atomic data for opacity calculations 13. Line-profiles for transitions in hydrogenic ions. *J. Phys. B: At. Mol. Opt. Phys.* **23**, 3255–3296.

Serduke, F.J.D., Mínguez, E., Davidson, S.J. & Iglesias, C.A. (2000). WorkOp-IV summary: Lessons from iron opacities. *J. Quant. Spectrosc. Radiat. Trans.* **65**, 527–541.

Skinner, C.H. & Federici, G. (2006). Is carbon a realistic choice for ITER's divertor? *Phys. Scr.* **T124**, 18–22.

Stewart, J.C. & Pyatt, K.D. Jr. (1966). Lowering of ionization potentials in plasmas. *Astrophys. J.* **144**, 1203–1211.

Van Regemorter, H.V. (1962). Rate of collisional excitation in stellar atmospheres. *Astrophys. J.* **136**, 906–915.

Winhart, G., Eidmann, K., Iglesias, C.A., Bar-Shalom, A., Mínguez, E., Rickert, A. & Rose, S.J. (1995). XUV opacity measurements and comparison with models. *J. Quant. Spectrosc. Radiat. Trans.* **54**, 437–446.

Wu, Z., Pang, J. & Yan, J. (2006). Opacity calculations for high-Z plasmas in non-local thermodynamic equilibrium. *J. Quant. Spectrosc. Radiat. Trans.* **102**, 402–408.

Yuan, J. & Moses, G.A. (2006). YAC: a code using the detailed accounting model for all-Z elements. *J. Quant. Spectrosc. Radiat. Trans.* **99**, 697–711.

Yuan, J., Haynes, D.A., Peterson, R.R. & Moses, G.A. (2003). Flexible database-driven opacity and spectrum calculations. *J. Quant. Spectrosc. Radiat. Trans.* **81**, 513–520.

Zeng, J. & Yuan, J. (2002). Detailed-term-accounting approximation calculations of the radiative opacity of aluminum plasma: a systematic study. *Phys. Rev. E* **66**, 0164011.

Zeng, J., Yuan, J. & Lu, Q. (2001*a*). Photoionization of O III low-lying states: autoionization resonance energies and widths of some 1s-2p excited states. *J. Phys. B: At. Mol. Opt. Phys.* **34**, 2823–2833.

Zeng, J., Yuan, J. & Lu, Q. (2001*b*). Detailed-term-accounting-approximation calculations of the radiative opacity of laser-produced Al plasmas. *Phys. Rev. E.* **64**, 0664121.